

Temperature dependence of resistivity of RFeAsO compounds

S. Mukherjee¹ · Papri Dasgupta² · Asok Poddar² · Chandan Mazumdar²

Received: 7 July 2015 / Accepted: 16 November 2015 / Published online: 15 December 2015
© The Author(s) 2015. This article is published with open access at Springerlink.com

Abstract The resistivity (ρ) data for RFeAsO compounds ($R = \text{Ce, Pr, Nd, Sm}$), in the temperature (T) range 35–315 K have been analyzed to identify the dominant scattering mechanisms. Close to the room temperature, the system appears to be a metal with low electron density, and the electron–phonon scattering is the dominant one. At lower temperatures, electron–electron scattering plays an important role. In an intermediate temperature region, unlike metallic system, $d\rho/dT$ is negative; and ρ^{-1} varies as $\ln T$ as in a state of weak localization. We look into the origin of negative $d\rho/dT$. The analysis of $\rho(T)$ data below the SDW transition temperature shows the presence of electron–electron interaction in addition to a SDW energy gap, and also gives an estimate of the SDW energy gap.

Keywords Oxy pnictides · Resistivity · Transport · Weak localization

Introduction

Extensive research work has been done on the oxy pnictides after the discovery of superconductivity in fluorine (F)-doped LaFeAsO by Kamihara et al. [1]. Interestingly, the superconducting compound contains the most familiar ferromagnetic atom “iron”, and the observed superconducting transition temperature (T_c) for LaFeAs(O_{0.89}F_{0.11})

is relatively high (26 K) [2]. Takahashi et al. reported that T_c of this compound rises to 43 K under a high pressure of $\approx 4\text{GPa}$ [3]. Subsequently, superconductivity has been reported in other RFeAs(O_{1-x}F_x) compounds with $R = \text{Ce, Pr, Nd, Sm, etc.}$, and the reported values of T_c are 41 K in CeFeAsO_{0.84}F_{0.16}, 52 K in PrFeAsO_{0.89}F_{0.11}, 54.3 K in NdFeAsO_{1-y}, 55 K in SmFeAsO_{0.9}F_{0.1}, and 54 K in GdFeAsO_{1-y} [4]. By now the iron-based superconductors have been extended to a much larger group containing variety of materials, mainly, four prototypical families 1111, 122, 111, and 11 types, and further variations such as 42622-type iron pnictides and 122-type iron chalcogenides [4].

RFeAsO compounds, with $R = \text{La}$ or rare earth elements belong to the 1111-type family. At room temperature, they are of ZrCuSiAs-type structure belonging to the tetragonal (T) $P4/nmm$ space group. The atomic structure consists of negatively charged Fe–As layers, and positively charged R–O layers. The structure may also be thought as a stacking of flat square nets of single atom types in the sequence 2O–R–As–2Fe–As–R. The layers are stacked along the c -axis, and such stacking of these layers gives tetrahedral coordination to Fe and O, while R and As are in square antiprismatic coordination [5, 6].

With the lowering of temperature, RFeAsO undergoes a structural phase transition (SPT) resulting into a stretching of the square Fe nets into rectangular nets, and the symmetry is reduced to orthorhombic (O) ($Cmma$ space group) in the low-temperature phase. Polycrystalline RFeAsO samples show a broad continuous SPT [7]. Subsequently, an antiferromagnetically ordered state is formed with stripe-like magnetic order of small moments on the Fe sites. Regarding the origin of this antiferromagnetic (AFM) order, there are two propositions. One group identifies this order with the spin-density wave (SDW) [8] driven by

✉ S. Mukherjee
sanseb68@yahoo.co.in

¹ Department of Physics, The University of Burdwan,
Golapbag, Burdwan, West Bengal 713 104, India

² Saha Institute of Nuclear Physics, 1/AF Bidhannagar,
Kolkata, West Bengal 700 064, India

Fermi surface nesting between the electron pockets at M point and hole pockets at Γ point based on band structural calculations, while the other group suggests that the AFM order originates from the short-range magnetic exchange coupling between local moments [9].

Neutron diffraction studies for polycrystalline LaFeAsO suggest that the compound undergoes SPT at $T_S = 155$ K, and a transition to an AFM state at $T_N = 137$ K with an ordered magnetic moment of $0.36(5) \mu_B$ [10]. Inelastic neutron scattering studies on polycrystalline LaFeAsO confirmed the presence of two-dimensional magnetic fluctuations even up to room temperature. Such fluctuations are expected to introduce dynamic disorder of the O/T mixed phase in an otherwise ordered T phase at temperatures above the SPT [11]. Elastic neutron scattering studies on single-crystalline LaFeAsO also concluded that the finite local O precursors appear to form at $T_S = 156$ K, although the O–T SPT occurs at 148 K. The SDW state is observed below $T_N = 140$ K with an ordered moment larger than the earlier mentioned value [11].

From neutron scattering studies of polycrystalline CeFeAsO samples, the SPT and SDW transition have been reported to occur near $T_S = 155$ K and $T_N = 140$ K, respectively [12], although the difference between T_S and T_N depends on the sample quality [13]. Specific heat data for CeFeAsO suggest that the onsets of SPT appear to be at the same temperature for both the single crystalline as well as poly crystalline sample; although the transition appears to be broader for the latter [13, 14]. For polycrystalline PrFeAsO (T_S, T_N) have been reported to be (153K, 127 K) [15], whereas the same is (142 K, 137 K) for single crystal of NdFeAsO [16]. For SmFeAsO (T_S, T_N) is (175 K, 140 K) [17]. The reported values of (T_S, T_N) for the measured samples can also be seen in Table 1.

The room temperature value of the resistivity and its behavior near room temperature for LaFeAsO suggest the material to be a metal with low carrier concentration [18]. In the temperature range (200–165 K), ρ increases with the lowering of temperature reaching a maximum around $T_\rho = 165$ K [18]. Similar behavior of increasing $\rho(T)$ with

the lowering of temperature down to almost 150 K has been observed for the polycrystalline samples of CeFeAsO, PrFeAsO, NdFeAsO [5] and SmFeAsO [9] although McGuire et al. [5] consider the temperature variation of $\rho(T)$ to be negligible in the tetragonal phase. Upon further cooling, $\rho(T)$ drops sharply. In essence, the earlier reported data in the absence of magnetic field suggest the following characteristics:

- ρ increases with the lowering of temperature down to a temperature T_ρ , irrespective of whether the sample is single crystalline or polycrystalline, indicating the property to be an intrinsic one for RFeAsO system [13].
- ρ versus T curve shows a cusp at T_ρ .
- ρ decreases rapidly below T_ρ .
- The peak in $d\rho/dT$ has been pointed out to be an excellent mark of T_N , whereas the anomaly in $d\rho/dT$ at T_S is difficult to identify [13].

In earlier studies of the T -dependence of ρ for RFeAsO system, focus was mainly on the SPT and the subsequent AFM transition, and the emphasis was more on to find a signature of the said transitions from the $\rho(T)$ curve. However, we feel, certain important points like the underlying cause behind the negative $d\rho/dT$ observed in this system just above T_ρ , and the role of different scattering mechanisms [the idea of which can be obtained from the functional dependence of $\rho(T)$] in different phases have not been given due consideration. This paper is basically to get a comprehensive idea about the different scattering mechanisms and their relative strengths in RFeAsO system from the functional dependence of ρ on T in different temperature regions. We also wish to have a fresh look into the origin of negative $d\rho/dT$, another important feature of $\rho(T)$ of such system, by comparing with a superlattice (SL) made of a (LaVO₃)[6 unit cells]/(SrVO₃)[1 unit cell] [19].

Experimental

The samples used in the measurement of resistance are the same as those used for the measurement of thermoelectric power in Ref. [20]. The samples were prepared using solid-state reaction technique from high purity (99.99 %) rare earth elements (R=Ce, Pr, Nd, Sm), As (chips), and Fe and Fe₂O₃ (powder). To obtain RFeAsO, we first prepared RAs by mixing stoichiometric amount of R and As chips inside glove box filled with inert Argon gas. The mixture was then sealed in an evacuated quartz tube, and given subsequent heat treatment at 900 °C with intermediate grindings inside the glove box. Prepared RAs were mixed with stoichiometric amounts of Fe and Fe₂O₃ and the mixture was pressed into pellets. The pellet obtained for each of the

Table 1 T_S (temperature corresponding to the structural phase transition), T_N (temperature corresponding to the SDW transition), T_ρ (temperature corresponding to the cusp of $\rho(T)$ curve) and the temperature corresponding to the peak of $d\rho/dT$ versus T curve [($d\rho/dT$)_{peak}]

Sample	T_S (K)	T_N (K)	T_ρ (K)	($d\rho/dT$) _{peak} (K)
CeFeAsO	155	140	152	137
PrFeAsO	153	127	165	144
NdFeAsO	142	137	164	138
SmFeAsO	175	140	161	133
GdFeAsO	135	133	157	125



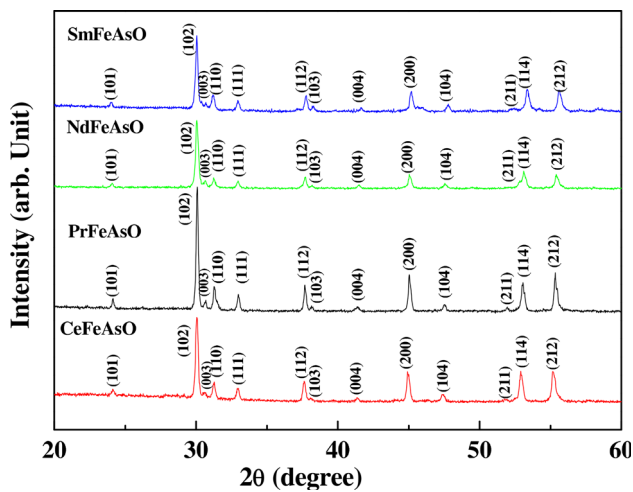


Fig. 1 Room temperature X-ray diffraction pattern for CeFeAsO, PrFeAsO, NdFeAsO and SmFeAsO

RFeAsO compounds was wrapped with Ta foil, and sealed in evacuated quartz tube. Finally, they were annealed at 1150–1200 °C for 48 h.

All the samples were characterized using powder X-Ray diffraction technique (PW/830, Philips, The Netherlands) with copper Cu K_{α} radiation at room temperature. Single phase natures of all the samples have been ascertained by indexing most of the peaks obtained in powder X-ray diffraction pattern (Fig. 1), assuming ZrCuSiAs-type (tetragonal) structure at room temperature (space group: $P4/nmm$). The standard four probe dc electrical resistivity measurements were performed using a close cycle refrigerator (25 K < T < 300).

Results and discussion

Figure 2 shows $\rho(T)$ for a number of members of the RFeAsO series, namely, CeFeAsO, PrFeAsO, NdFeAsO and SmFeAsO, all polycrystalline in nature, in the temperature range (35–315 K). The overall behavior of $\rho(T)$ for each sample is similar to the earlier reported data for RFeAsO [5, 9, 18], i.e., $\rho(T)$ increases with the lowering of temperature down to a temperature T_{ρ} (temperature corresponding to the cusp of $\rho(T)$ curve), and it decreases rapidly below the cusp at T_{ρ} . T_{ρ} for each sample has been given in Table 1.

For all of our samples belonging to the RFeAsO series, $\rho(T)$ shows metallic behavior with positive $d\rho/dT$ in a temperature region (Figs. 3, 4) close to room temperature. Figure 4 shows the behavior of $d\rho/dT$ for all of our samples in two temperature regions separately: a) 77 K—close to T_{ρ} (left panel), and b) temperature above T_{ρ} —room temperature (right panel). The range of temperature covering

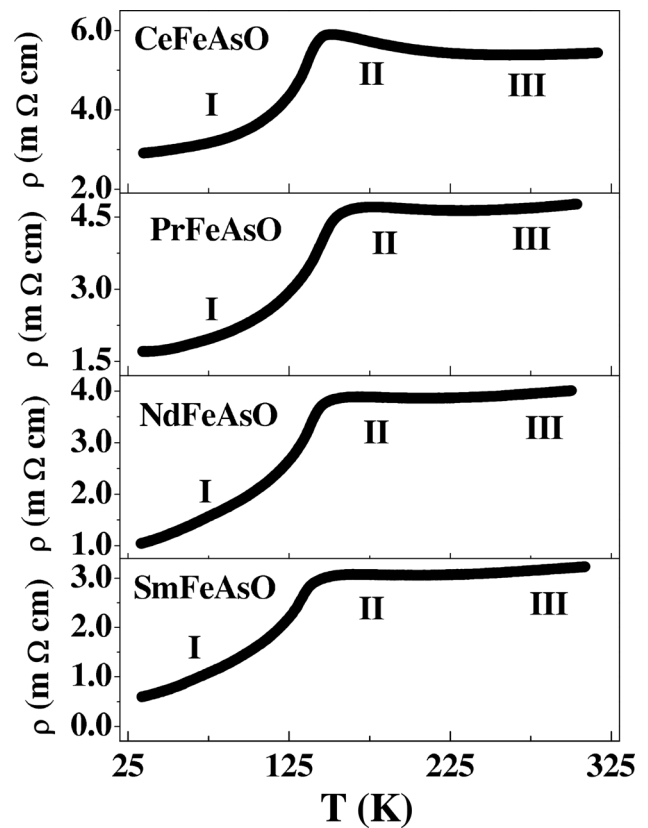


Fig. 2 Resistivity ρ as a function of temperature T for CeFeAsO, PrFeAsO, NdFeAsO, SmFeAsO

the linear region III (Fig. 3), the value of resistivity at 300 K ($\rho_{300\text{ K}}$) and the value of $d\rho/dT$ in this region III are shown in Table 2 for each of our sample. In region III, $d\rho/dT$ is of the order of $\mu\Omega\text{ cm/K}$.

The negative and temperature-independent value of the Hall coefficient as well as the negative value of thermoelectric power (S) near room temperature for RFeAsO system identify electron as the charge carrier in this region [18]. The estimated Fermi energy E_F is 0.19 eV [20]. The linear dependence of $\rho(T)$ on T can be obtained from the Bloch–Grüneisen formula for metals,

$$\rho(T) = \rho(0) + A(T/\theta_R)^5 \int_0^{\theta_R/T} \frac{x^5}{(e^x - 1)(1 - e^{-x})} dx$$

as a high-temperature limit, i.e., at temperatures above the Debye temperature θ_R considering the resistance is due to scattering of electrons by phonons. The Debye temperatures for members of RFeAsO series are close to room temperature [21]. Hence, in the region III, the dominant scattering mechanism is the electron–phonon one.

From Fig. 4, we observe for each of our sample that in an intermediate temperature range (region II of Fig. 2, the range depends upon the choice of the element R) unlike

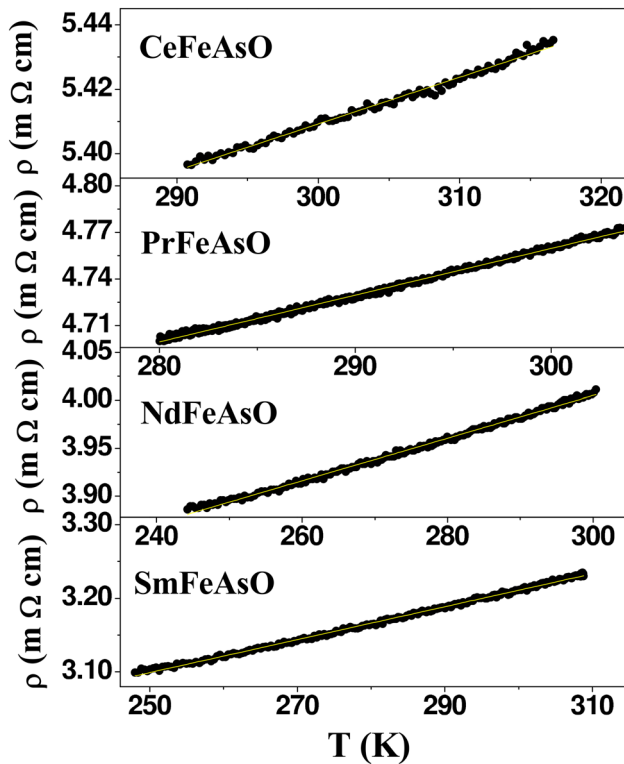


Fig. 3 $\rho(T)$ for all the samples in the region III, along with the fitted curves (solid line); ρ varies linearly with T

metallic system, $d\rho/dT$ is negative, although small. Opening of a gap with the lowering of temperature might cause such negative $d\rho/dT$. However, the weak temperature dependence in this region discards the possibility of opening a gap, and rather it suggests the system to be still in metallic phase with a loss of charge carrier coherence [19]. For polycrystalline LaFeAsO, such a negative $d\rho/dT$ below 200 K has been conjectured to be due to the increased charge carrier scattering by lattice fluctuations related to the onset of SPT [18]. Similar observation of negative $d\rho/dT$ above the SPT temperature in case of a superlattice (SL) made of a $(\text{LaVO}_3)[6 \text{ unit cells}]/(\text{SrVO}_3)[1 \text{ unit cell}]$ [19], and their analysis encourages us to think in a different way. Moreover, it may also be noted that RFeAsO and the SL have following interesting points of similarities:

1. In both the systems, the conducting zones are of two-dimensional (2D) characters. In the SL, a single unit cell of SrVO_3 is introduced between the insulating LaVO_3 layers, whereas in RFeAsO the conducting layers of $(\text{FeAs})^-$ are interlaced by the insulating layers of $(\text{RO})^+$.
2. In RFeAsO, we find SPT around $T_S = 150 \text{ K}$, and likewise the SL undergoes a SPT at $T_S = 130 \text{ K}$ from

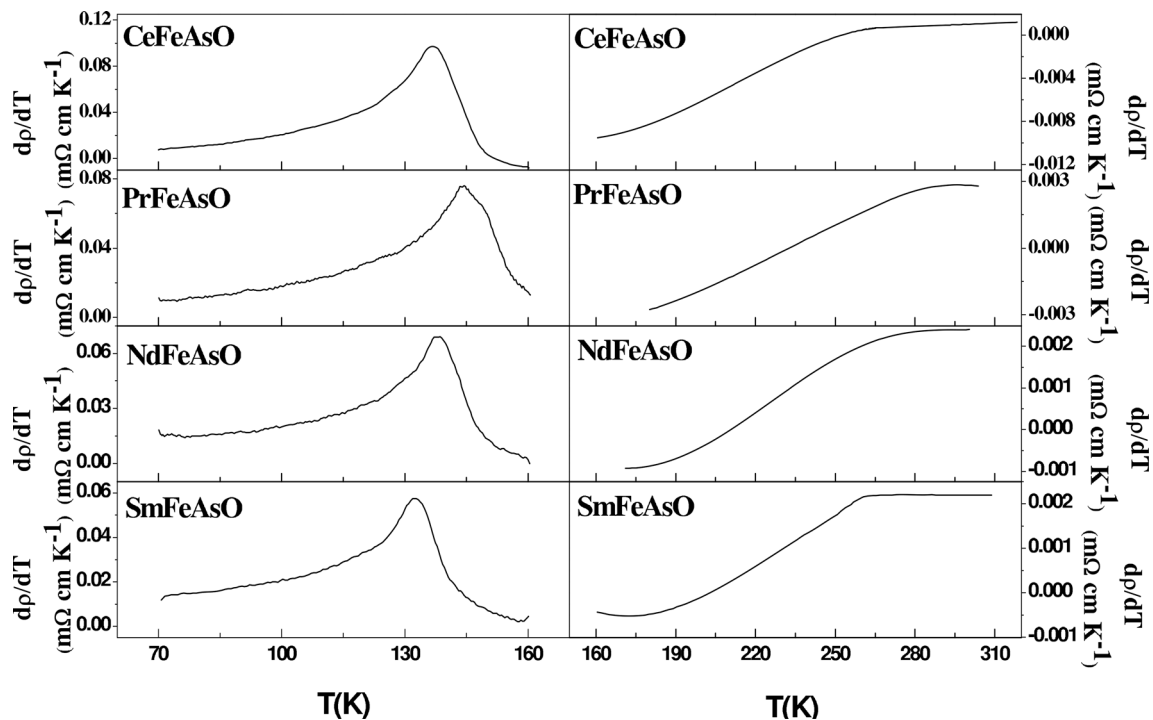


Fig. 4 $d\rho/dT$ as a function of temperature T : left panel covers the region (60–160 K), while the right panel describes the region (160–315 K) for each sample

Table 2 Temperature range corresponding to regions I, II & III; measured ρ at 300 K (ρ_{300K}), earlier reported values of ρ at 300 K (ρ_{300K} (reported)), value of $d\rho/dT$ in region III and the SDW energy gap Δ

Sample	Region III ^a (K)	ρ_{300K} (m Ω cm)	ρ_{300K} (reported) (m Ω cm)	$d\rho/dT$ (m Ω cm/K)	Region II (K)	Region I (K)	Δ (K)
CeFeAsO	250–318	5.4	4.9 [11]	8.4×10^{-4}	160–235	34–141	964
PrFeAsO	270–307	4.8	4.3 [5]	2.8×10^{-3}	175–235	34–148	968
NdFeAsO	244–301	4	3.3 [5]	2.2×10^{-3}	164–212	34–140	965
SmFeAsO	248–311	3.2	3.0 [28]	2.2×10^{-3}	164–211	34–138	968
GdFeAsO	201–312	6.0	2.4 [16]	4.2×10^{-3}	157–183	34–128	975

^a Temperature range is taken from the linearly fitted region of Fig. 1

- a high-temperature tetragonal phase to a low-temperature monoclinic one.
- 3. The value of the room temperature resistivity for both the systems corresponds to poor metals.
- 4. In both the cases, $d\rho/dT$ is negative and low indicating weak temperature dependence above T_S , and the same is positive and high below T_S .

In the SL, the negative $d\rho/dT$ above T_S has been explained by the weak localization in 2D. Physically, weak localization is the interference of pairs of waves into which conduction electrons split in the backscattering direction. Resistance is a measure of the intensity of interference. In the state of “weak localization” ρ^{-1} varies as $\ln T$. For a number of two-dimensional systems such as thin films of Pd, Pt or Au alloys, such logarithmic increase of resistance has been interpreted as weak localization [22].

Figure 5 shows that the region II for each of our sample is well described by a linear variation of $1/\rho$ with $\ln T$. The temperature range of this region has been noted in Table 2. This motivates us to conclude that the weak localization in 2D is responsible for such behavior like the mentioned SL [19]. However, such temperature dependence alone can not conclude decisively the state of weak localization. On the other hand, a similar behavior of resistivity ($1/\rho - \ln T$) at low temperature in disordered 2D electron systems can be observed due to modified electron–electron (Coulomb) interaction also [22]. These two cases can be differentiated by performing the measurements in the presence of a magnetic field. In the state of weak localization, in which the conduction electrons split into pairs of interfering waves, application of a magnetic field (H) introduces a phase shift in the electronic wave function and suppresses the interference after a time interval proportional to $1/H$ [22]. Therefore, the magneto resistive (MR) effect should be dominant in this state. On the other hand, the MR of the second case which owes its origin to the Coulomb interaction is either negligible or only present in large fields. However, unlike the SL, for RFeAsO, the MR is negligible in this temperature range, although it is significant at temperatures below the SPT [23]. The MR is less

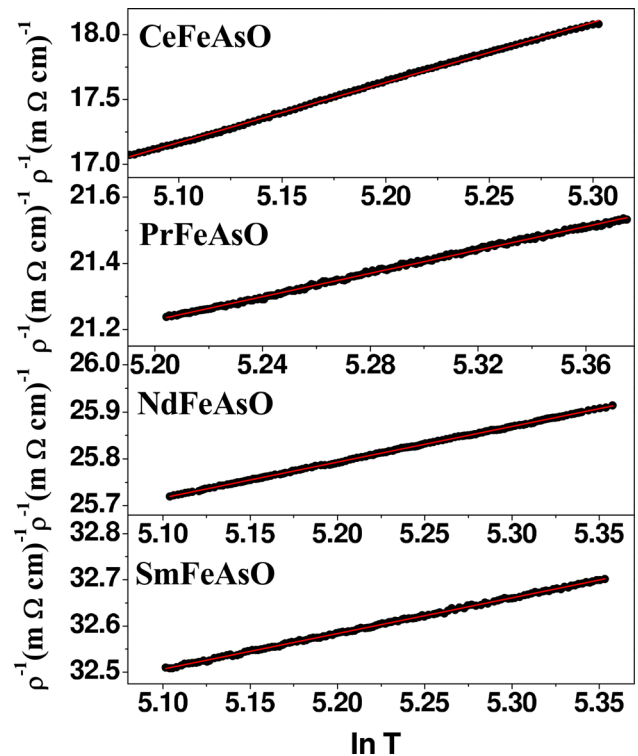


Fig. 5 $\rho^{-1} \ln T$ in the region II for all the samples; curves a linear variation of $1/\rho$ with $\ln T$ in this region

than 2 % for both SmFeAsO and PrFeAsO even in a field of $14 T$ at a temperature higher than $150 K$ [24] although a negative longitudinal in-plane MR has been observed in different $Ba(Fe_{1-x}Co_x)_2As_2$ single crystals in the paramagnetic phase [25]. Moreover, the localization theory deals with the noninteracting electrons [22], whereas the presence of strong electron–electron scattering in this intermediate temperature range has been predicted in RFeAsO systems [20]. Our study of temperature dependence of resistivity also confirms such observation, and we feel that electron–electron scattering is responsible for linear variation of $1/\rho$ with $\ln T$ in region II.

For the range of temperatures below the SDW transition, Cheng et al. [26] have analyzed their resistivity data with the functional dependence $\rho(T) = \rho_0 + AT^2 + BT(1 +$

$2T/\Delta)\exp(-\Delta/T)$; ρ_0 is the residual resistivity, A and B are the fitting parameters. The second term containing the T^2 term describes the Fermi liquid behavior, while the last term signifies the metallic ferromagnetic or antiferromagnetic state with an energy gap Δ . The associated theory has been given by Anderson and Smith [27]. The region I of each curve of Fig. 1 has been shown separately in Fig. 6, and fitted with the mentioned expression. The range of temperature, corresponding to region I for each sample has been noted in Table 2. In each case, the fitted parameter Δ which is a measure of the SDW energy gap has been given in Table 2. The SDW energy gap has been found to be of the order of 1000 K for any member of the RFeAsO series and comparable to the reported value of 1082 K for NdFeAsO single crystal [26].

$d\rho/dT$ for LaFeAsO shows a peak at 143 K, closer to the SDW transition temperature than T_S [18]. On the other hand, in the Ref. 5, $d\rho/dT$ has been claimed to show double-peaked structure for the samples CeFeAsO, PrFeAsO, NdFeAsO in addition to LaFeAsO. In explaining such double-peaked structure, one of the overlapping peaks has been associated with the crystallographic distortion and the

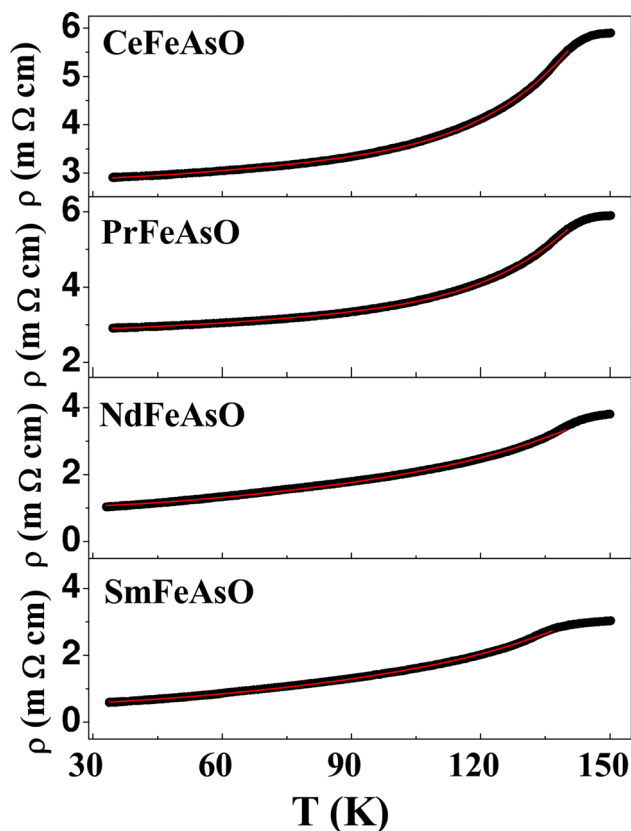


Fig. 6 $\rho(T)$ for all the samples in the region I, along with fitted curves, which show $\rho(T)$ varies as $\rho_0 + AT^2 + BT(1 + 2T/\Delta)\exp(-\Delta/T)$

other with the magnetic ordering [5]. On the other hand, Luo et al. [9] report single peak in each of the $d\rho/dT$ versus T curves for polycrystalline LaFeAsO, SmFeAsO and GdFeAsO. The respective peak temperatures 132, 133, 128 K have been pointed out to be closer to AFM ordering temperatures rather than the SPT temperatures. For each of our samples, $d\rho/dT$ shows peak at a single temperature (Fig. 4). The peak temperatures $(d\rho/dT)_{\text{peak}}$ are noted in Table 1. $(d\rho/dT)_{\text{peak}}$ appears to be closer to T_{SDW} than T_S . Reported value of $\rho_{300\text{K}}$ for SmFeAsO mentioned in Table 2 has been taken from Ref. [28].

Conclusion

The overall behavior of $\rho(T)$ for any of our sample is identical to the earlier reported data. The whole temperature range of measurement can be divided into three regions. In the region III, close to room temperature, the system behaves as a metal with low carrier (electron) density, and the electron–phonon scattering is dominant. In the intermediate region II, $(d\rho/dT)$ is negative, and ρ^{-1} varies as $\ln T$. Such a behavior cannot be explained by weak localization in absence of MR effect, rather electron–electron interaction appears to be responsible. Below the SDW transition temperature, the contribution to resistivity comes from electron–electron interaction, signified by a term proportional to T^2 in presence of SDW energy gap. The energy gap for the system has been identified to be of the order of 1000 K. $(d\rho/dT)$ for any of our samples shows a single peak at a temperature closer to T_{SDW} than T_S .

Acknowledgments Dr. Papri Dasgupta working as women scientist under Department of Science and Technology (DST), India for the project SR/WOS-A/PS-38/2013 acknowledges DST for financial support.

Open Access This article is distributed under the terms of the Creative Commons Attribution 4.0 International License (<http://creativecommons.org/licenses/by/4.0/>), which permits unrestricted use, distribution, and reproduction in any medium, provided you give appropriate credit to the original author(s) and the source, provide a link to the Creative Commons license, and indicate if changes were made.

References

1. Kamihara, Y., Watanabe, T., Hirano, M., Hosono, H.: Iron-based layered superconductor $\text{La}[\text{O}_{1-x}\text{F}_x]\text{FeAs}$ ($x = 0.05 - 0.12$) with $T_c = 26$ K. *J. Am. Chem. Soc.* **130**, 3296 (2008)
2. Ishida, K., Nakai, Y., Hosono, H.: To what extent iron-pnictide new superconductors have been clarified: a progress report. *J. Phys. Soc. Jpn.* **78**, 062001 (2009)
3. Takahashi, H., Igawa, K., Arii, K., Kamihara, Y., Hirano, M., Hosono, H.: Superconductivity at 43 K in an iron-based layered compound $\text{LaO}_{1-x}\text{F}_x\text{FeAs}$. *Nature* **453**, 376–378 (2008)

4. Oh, H., Moon, J., Shin, D., Moon, C.-Y., Choi, H.J.: Prog. Supercond. **13**, 65 (2011)
5. McGuire, M.A., Hermann, R.P., Sefat, A.S., Sales, B.C., Jin, R., Mandrus, D., Grandjean, F., Long, G.J.: Influence of the rare-earth element on the effects of the structural and magnetic phase transitions in CeFeAsO, PrFeAsO and NdFeAsO. New J. Phys. **11**, 025011 (2009)
6. Lee, C.H., Kihou, K., Iyo, A., Kito, H., Shirage, P.M., Eisaki, H.: Relationship between crystal structure and superconductivity in iron-based superconductors. Solid State Commun. **152**, 644–648 (2012)
7. Ricci, A., Poccia, N., Joseph, B., Barba, L., Arrighetti, G., Ciasca, G., Yan, J.-Q., McCallum, R.W., Lograsso, T.A., Zhigadlo, N.D., Karpinski, J., Bianconi, A.: Structural phase transition and superlattice misfit strain of RFeAsO (R=La, Pr, Nd, Sm). Phys. Rev. B **82**, 144507 (2010)
8. Pan, M., Huang, Z., Cheng, C.H., Zhao, Y.: Possible coexistence of SDW state with superconductivity in Ir doped SmOFeAs. Solid State Commun. **152**, 458–461 (2012)
9. Luo, Y., Tao, Q., Li, Y., Lin, X., Li, L., Cao, G., Xu, Z., Xue, Y., Kaneko, H., Savinkov, A.V., Suzuki, H., Fang, C., Hu, J.: Evidence of magnetically driven structural phase transition in RFeAsO (R=La, Sm, Gd, and Tb): a low-temperature x-ray diffraction study. Phys. Rev. B **80**, 224511 (2009)
10. dela Cruz, C., Huang, Q., Lynn, J.W., Li, J.Y., Ratcliff, W., Zarestky, J.L., Mook, H.A., Chen, G.F., Luo, J.L., Wang, N.L., Dai, P.C.: Magnetic order close to superconductivity in the iron-based layered LaO_{1-x}FxFeAs systems. Nat. (Lond.) **453**, 899–902 (2008)
11. Li, H.-F., Tian, W., Yan, J.-Q., Zarestky, J.L., McCallum, R.W., Lograsso, T.A., Vaknin, D.: Phase transitions and iron-ordered moment form factor in LaFeAsO. Phys. Rev. B **82**, 064409 (2010)
12. Zhao, J., Huang, Q., de la Cruz, C., Li, S., Lynn, J.W., Chen, Y., Green, M.A., Chen, G.F., Li, G., Li, Z., Luo, J.L., Wang, N.L., Dai, P.: Structural and magnetic phase diagram of CeFeAsO_{1-x}F_x and its relation to high-temperature superconductivity. Nat. Mater. **7**, 953–959 (2008)
13. Jesche, A., Krellner, C., de Souza, M., Lang, M., Geibel, C.: Coupling between the structural and magnetic transition in CeFeAsO. Phys. Rev. B **81**, 134525 (2010)
14. Zocco, D.A., Baumbach, R.E., Hamlin, J.J., Janoschek, M., Lum, I.K., McGuire, M.A., Sefat, A.S., Sales, B.C., Jin, R., Mandrus, D., Jeffries, J.R., Weir, S.T., Vohra, Y.K., Maple, M.B.: Search for pressure-induced superconductivity in CeFeAsO and CeFePO iron pnictides. Phys. Rev. B **83**, 094528 (2011)
15. Zhao, J., Huang, Q., de la Cruz, C., Lynn, J.W., Lumsden, M.D., Ren, Z.A., Yang, J., Shen, X., Dong, X., Zhao, Z., Dai, P.: Lattice and magnetic structures of PrFeAsO, PrFeAsO_{0.85}F_{0.15}, and PrFeAsO_{0.85}. Phys. Rev. B **78**, 132504 (2008)
16. Tian, W., Ratcliff, W., Kim, M.G., Yan, J.-Q., Kienzle, P.A., Huang, Q., Jensen, B., Dennis, K.W., McCallum, R.W., Lograsso, T.A., McQueeney, R.J., Goldman, A.I., Lynn, J.W., Kreyssig, A.: Interplay of Fe and Nd magnetism in NdFeAsO single crystals. Phys. Rev. B **82**, 060514(R) (2010)
17. Martinelli, A., Palenzona, A., Tropeano, M., Putti, M., Ferdeghini, C., Profeta, G., Emerich, E.: Retention of the tetragonal to orthorhombic structural transition in F-substituted SmFeAsO: a new phase diagram for SmFeAs(O_{1-x}F_x). Phys. Rev. Lett. **106**, 227001 (2011)
18. McGuire, M.A., Christianson, A.D., Sefat, A.S., Sales, B.C., Lumsden, M.D., Jin, R., Payzant, E.A., Mandrus, D., Luan, Y., Keppens, V., Varadarajan, V., Brill, J.W., Hermann, R.P., Sougrati, M.T., Grandjean, F., Long, G.J.: Phase transitions in LaFeAsO: Structural, magnetic, elastic, and transport properties, heat capacity and Mössbauer spectra. Phys. Rev. B **78**, 094517 (2008)
19. David, A., Frésard, R., Boullay, Ph, Prellier, W., Lüders, U., Janolin, P.E.: Structural transition in LaVO₃/SrVO₃ superlattices and its influence on transport properties. Appl. Phys. Lett. **98**, 212106 (2011)
20. Poddar, A., Mukherjee, S., Samanta, T., Saha, R.S., Mukherjee, R., Dasgupta, P., Mazumdar, C., Ranganathan, R.: Thermoelectric power of RFeAsO (R=Ce, Pr, Nd, Sm and Gd). Phys. C **469**, 789–794 (2009)
21. Kaurav, N., Chung, Y.T., Kuo, Y.K., Liu, R.S., Chan, T.S., Chen, J.M., Lee, J.-F., Sheu, H.-S., Wang, X.L., Dou, S.X., Lee, S.I., Shi, Y.G., Belik, A.A., Yamaura, K., Takayama-Muromachi, E.: Crystal structure and electronic and thermal properties of TbFeAsO_{0.85}. Appl. Phys. Lett. **94**, 192507 (2009)
22. Bergmann, G.: Consistent temperature and field dependence in weak localization. Phys. Rev. B **28**, 515 (1983)
23. Yuan, H.Q., Jiao, L., Singleton, J., Balakirev, F.F., Chen, G.F., Luo, J.L., Wang, N.L.: The magnetoresistance and Hall effect in CeFeAsO: a high magnetic field study. J. Phys. Conf. Ser. **273**, 012110 (2011)
24. Meena, R.S., Singh, S.K., Pal, A., Kumar, A., Jha, R., Rao, K.V.R., Du, Y., Wang, X.L., Awana, V.P.S.: High field (14 T) magneto transport of Sm/PrFeAsO. J. Appl. Phys. **111**, 07E232–07E233 (2012)
25. Rullier-Albenque, F., Colson, D., Forget, A.: Longitudinal magnetoresistance in Co-doped BaFe₂As₂ and LiFeAs single crystals: interplay between spin fluctuations and charge transport in iron pnictides. Phys. Rev. B **88**, 045105 (2013)
26. Cheng, P., Yang, H., Jia, Y., Fang, L., Zhu, X., Mu, G., Wen, H.-H.: Hall effect and magnetoresistance in single crystals of NdFeAsO_{1-x}F_x (x = 0 and 0.18). Phys. Rev. B **78**, 134508 (2008)
27. Andersen, N.H., Smith, H.: Electron-magnon interaction and the electrical resistivity of Tb. Phys. Rev. B **19**, 384–387 (1979)
28. Tropeano, M., Fanciulli, C., Ferdeghini, C., Marrè, D., Siri, A.S., Putti, M., Martinelli, A., Ferretti, M., Palenzona, A., Cimberle, M.R., Mirri, C., Lupi, S., Sopracase, R., Calvani, P., Perucchi, A.: Transport and infrared properties of SmFeAs(O_{1-x}F_x): from SDW to superconducting ordering. Supercond. Sci. Technol. **22**, 034004 (2009)

